Fusion of Multiple-Look Synthetic Aperture Radar Images at Data and Image Levels

Ram M. Narayanan, Zhixi Li, and Scott Papson
Dept. of Electrical Engineering, Pennsylvania State University, University Park, PA 16802, USA
Phone (+1) 814-863-2602 Fax (+1) 814-865-7065 E-mail: ram@engr.psu.edu

Abstract — **Synthetic aperture radar (SAR) and inverse synthetic aperture radar (ISAR) have proven capabilities for non-cooperative target recognition (NCTR) applications. Multiple looks of the same target (at different aspect angles, frequencies, etc.) can be exploited to enhance target recognition by fusing the information from each look. Such fusion can be performed at the raw data level or at the processed image level depending on what is available. At the data level, physics based image fusion techniques can be developed by processing the raw data collected from multiple inverse synthetic aperture radar (ISAR) sensors, even if these individual images are at different resolutions. The technique maps multiple data sets collected by multiple radars with different system parameters on to the same spatial-frequency space. The composite image can be reconstructed using the inverse 2-D Fourier Transform over the separated multiple integration areas. An algorithm called the Matrix Fourier Transform (MFT) is proposed to realize such a complicated integral. At the image level, a persistence framework can be used to enhance target features in large, aspect-varying datasets. The model focuses on cases containing rich aspect data from a single depression angle. The goal is to replace the data's intrinsic viewing geometry dependencies with target-specific dependencies. Both direct mapping functions and cost functions are presented for data transformation. An intensity-only mapping function is realized to illustrate the persistence model in terms of a canonical example, visualization, and classification.**

Keywords — **persistence model, image fusion, data fusion, SAR, ISAR, Matrix Fourier Transform.**

I. Introduction and Background

In this paper, we address two new approaches for integration of outputs obtained from high-resolution radar sensors at multiple locations or multiple aspects, including sensors operating at different frequencies at different resolutions, and even radars of opportunity. This is similar to the concept of netted radars wherein additional target information is gathered and processed using data from radars at different locations for better definition of target features and characteristics. With accurate location and time data, multiple radar outputs can be integrated together, either using raw or processed data, to form composite radar images combining the best features from the individual radar images. When combining raw radar data, we use the Matrix Fourier Transform approach, while processed images are combined using the image persistence model.

In inverse synthetic aperture radar (ISAR), the synthetic aperture is achieved by the coherent processing of reflectivity data collected from the changing observation angles presented during target illumination. The relative motion needed to obtain the synthetic aperture can be decomposed into translational motion and rotational motion. There are numerous papers dealing with the translational motion compensation for the purpose of improving the image resolution and reducing image blurring, and this aspect is not treated here. Supposing that the translational motion has been accurately compensated, the target can be treated as a rotating object with respect to the auto-focusing center. The rotation of an ISAR target can be roughly categorized into the following three classes: (i) uniform planar rotation with a constant angular velocity, (ii) non-uniform planar rotation with a time variant angular velocity, and (iii) three-dimensional rotation with pitch, roll, and yaw [1]. For the first class, the Range-Doppler (RD) algorithm or specific preprocessing methods can be used to form a focused ISAR image [2], [3]. Fine down-range resolution is obtained by transmitting a signal that has a wide frequency bandwidth for ISAR. Doppler frequency resolution, and hence cross-range resolution, is proportional to the size of the synthesized antenna aperture. For the second class, interpolation or time-frequency techniques are two widely used methods to achieve a focused ISAR image [1], [4]. For the third class, the Doppler frequency of each scatterer is time-varying, because the maneuvering target's rotational velocity and axis vary with time. In this case, the time-frequency analysis is used to obtain Range-Instantaneous Doppler (RID) images, and imaging problem becomes an instantaneous Doppler parameter estimation problem. A number of estimation methods and imaging methods have been proposed, such as, joint time-frequency method [5], [6], Radon-Wigner method [7], chirplet decomposition method [8], Extended Weighted RELAX method [1], etc. A recently emerging target recognition technique is the use of data from multiple radar systems, especially radars operating from multiple locations. This is similar to the concept of netted radars [9]. With accurate location and time data, these multiple radar images are processed together to form a composite radar image combining the best attributes of the individual images. Current fusion techniques tend to focus on general intensity image processing without using any ISAR imaging characteristics. Our specific radar image fusion algorithm fills this important gap. In our research, a data-level algorithm is developed for the multi-location ISAR image fusion. Instead of processing individual images, this approach executes the data fusion algorithms at the raw radar signal level first. The signal information is fused

IEEE Catalog Number: CFP08827-CDR
ISBN: 978-1-4244-2499-3
Library of Congress: 2008903800

directly and then subsequently processed to produce the resulting ISAR image. This model is based on coordinate transformation, and implements the Matrix Fourier Transform (MFT) method developed by us. The fusion algorithm guarantees that individual data sets collected from multiple aspects can be combined without losing any phase information. All simulations are based on the actually measured ISAR database, namely, the ERADS Slicy database. Slicy is the name given to a composite metallic target comprised of a variety of simple shapes, such as dihedrals, trihedrals, and cylinders on a rectangular base.

Synthetic aperture radar (SAR) is a well established methodology for automated target recognition (ATR) applications. However as sensor automation and processing power have increased, the paradigm has shifted from a single-aspect per target to systems with multiple images over varied aspects or continued surveillance of critical targets. In this multi-aspect space, new opportunities and challenges emerge. Although the traditional method of ordering a set of multi-aspect images as a function of the aspect angle is intuitively appealing, there are some fundamental limitations to this approach. Instead, researchers are looking for methods to generate either a single image or sets of images that have target specific features [10, 11]. The work spans from theoretical three-dimensional image formulation, to data and classification fusion. For example, in the presence of circular apertures at multiple elevations, three dimensional target images can be formed [12, 13]. Similarly, techniques have been developed for the formation of single two-dimensional images from coherent data collected via a perfectly circular aspect [13]. In many battle spaces, however, such large and well-formed datasets are not available. Instead only a subset of that data may be available or the data may have been collected from multiple platforms and cannot easily be coherently fused. On the other end of the spectrum, there are techniques that treat multiple images as isolated and input them independently into various ATR algorithms. There is also a large body of work where SAR images are fused across aspect, resolution, and even frequency. The goal of the persistence modeling technique presented in this paper is to bridge the gap between theoretical image formulation and practical applications in ATR. The proposed persistence model uses images from multiple aspects or sub-apertures to create a new set of target images that capture the desired characteristics. We develop and present a framework for the treatment of SAR images that balances data integration, image fusion, feature extraction, and other relevant processes. DARPA's Moving and Stationary Target Acquisition and Recognition (MSTAR) database [14] is used to show the application of the persistence modeling approach to real-world data. The dataset contains spotlight SAR images at 1-foot resolution and a range of 5000 meters.

II. Problem Formalism

A. Fusion Based on the Matrix Fourier Transform

Assume there is a two-dimensional target with arbitrary shape rotating with angle extension Θ under rotation class (i) mentioned in the Introduction, and that there are two radars ISAR1 and ISAR2 viewing the target at the same time. The geometry is shown in Fig. 1. The returned baseband signal of ISAR1, ignoring the amplitude term, can be expressed as

$$G_1(f,\theta)=\int_{-\infty}^{\infty}\int_{-\infty}^{\infty}\rho(x,y)\exp[j2\pi(xf_x+yf_y)]dxdy \qquad (1)$$

where $f_x = -(2/\lambda_1)\sin\theta$ and $f_y = (2/\lambda_1)\cos\theta$ are the spatial-frequency quantities defined at the radar transmit frequency f_1 and target rotation angle θ, and $\rho(x,y)$ is the two-dimensional reflectivity density function of the target. The baseband phase signal of ISAR2, which is apart from ISAR1 by an intra-angle β, has a similar form, given by

$$G_2(f,\theta)=\int_{-\infty}^{\infty}\int_{-\infty}^{\infty}\rho(u,v)\exp[j2\pi(uf_u+vf_v)]dudv \qquad (2)$$

where $f_u = -(2/\lambda_2)\sin\theta$ and $f_v = (2/\lambda_2)\cos\theta$. It is represented in another rectangular coordinate system, although both ISARs are looking at the same object space.

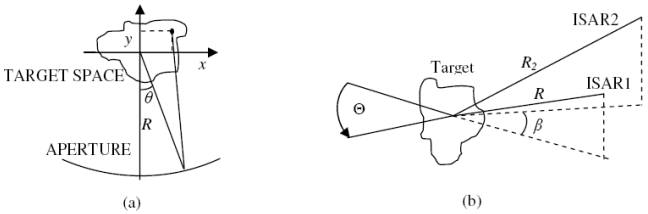

Fig. 1. ISAR geometry: (a) Single ISAR, (b) Multiple ISARs.

These two 2-D coordinate systems are also apart from each other by the same intra-angle β as shown in Fig. 2(a) for which the coordinate transformation relationship is:

$$\begin{cases} u = x\cos\beta + y\sin\beta \\ v = y\cos\beta - x\sin\beta \end{cases}. \qquad (3)$$

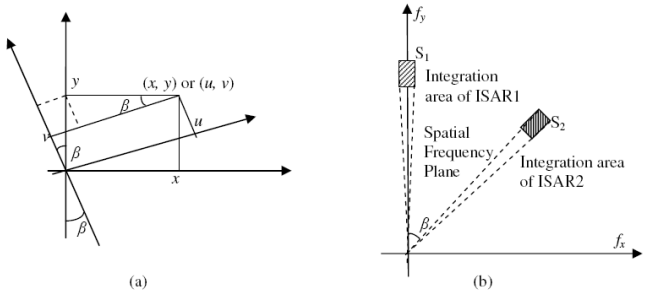

Fig. 2. Derivation of the data fusion rule: (a) Coordinate transformation, (b) Integration areas for multi-location wideband ISARs in spatial frequency domain.

Substituting (3) into (2), and some rearrangement, we obtain

IEEE Catalog Number: CFP08827-CDR
ISBN: 978-1-4244-2499-3
Library of Congress: 2008903800

$$G_2(f,\theta)=\int_{-\infty}^{\infty}\int_{-\infty}^{\infty}\rho(x,y)\exp\{j\frac{4\pi f_2}{c}\cdot [y\cos(\theta+\beta)-x\sin(\theta+\beta)]\}dxdy \quad (4)$$

Equation (4) indicates that the data obtained by ISAR2 can be mapped onto the Spatial-Frequency space built by ISAR1, but they are located in different regions: the two data regions are separated by angle β, as shown in Fig. 2(b). Both S_1 and S_2 are sectors, but they are approximately rectangular when Θ is small. Traditionally, the inverse Fast Fourier Transform (FFT) is used to reconstruct the image. The ideal Fourier integration area should be the entire Spatial-Frequency plane. However, it is limited by the radar bandwidth and number of samples. Theoretically, the larger the integration area, the better is the image quality. If we integrate the available data over two or more patches instead of only one, the integration area will be expanded, and thus the image quality will be improved. The data fusion rule for multi-location ISARs transmitting wideband signals can be represented as:

$$g'(x,y)=\iint_{S_1}G_1(f,\theta)\exp[-j2\pi(xf_x+yf_y)]df_x df_y + \iint_{S_2}G_2(f,\theta)\exp[-j2\pi(xf_x+yf_y)]df_x df_y \quad (5)$$

The data fusion rule contains the Fourier transform over two separated sectors, which requires robust and accurate data interpolation. But interpolation is usually not lossless. In [15], the authors proposed a data interpolation algorithm which could accurately obtain uniformly spaced data from the available arbitrarily distributed data samples within the same data range. The principle of this method is based on the independency between the data in the spatial domain and frequency domain, i.e., even though data samples f_x and f_y are arbitrarily distributed, x_i and y_j can be chosen to be uniformly spaced during the Fourier Transform. However, the intervals over the frequency samples chosen by the authors are not directly applicable to the data fusion rule because they are much larger than the ISAR image resolutions. Thankful for the independency property, we can choose the frequency resolutions (in our case, they are the spatial resolutions) to match the system parameters. Now, the 2-D Fourier transform required by the data fusion rule can be accomplished by a matrix-based calculation, which we call the Matrix Fourier Transform (MFT):

First, equation (5) is rewritten in the form of a discrete 2-D Fourier transform as shown below:

$$g'(x_i,y_j)=\sum_{m=1}^{N_f}\sum_{n=1}^{N_\theta}\left(\begin{matrix}G_1(f_m,\theta_n)\exp[-j2\pi f_x(f_m,\theta_n)\cdot x_i+\\ j2\pi f_y(f_m,\theta_n)\cdot y_j]\end{matrix}\right) + \sum_{m=1}^{N_f}\sum_{n=1}^{N_\theta}\left(\begin{matrix}G_2(f_m,\theta_n)\exp[-j2\pi f_u(f_m,\theta_n)\cdot x_i+\\ j2\pi f_v(f_m,\theta_n)\cdot y_j]\end{matrix}\right) \quad (6)$$

Then, each spatial resolution cell (x_i, y_j) is selected to be at:

$$x_i=(-\frac{N_\theta}{2}+i-1)\cdot\Delta r_c \qquad y_j=(-\frac{N_f}{2}+j-1)\cdot\Delta r_s \quad (7)$$

where $i = 1, 2, \ldots, N_\theta$ and $j = 1, 2, \ldots, N_f$. Furthermore, N_f is the number of frequency bins, N_θ is the number of pulses during observation, and both are even. Δr_s is the range (i.e., down-range) resolution, and Δr_c is the cross-range resolution of the image. Substituting (7) into (6), changing the summation calculation to a matrix multiplication, and performing some rearrangement, we can realize the MFT.

B. Fusion Based on the Persistence Modeling Approach

Traditionally, ATR algorithms for SAR systems operate as a function of the target aspect angle since radar images will change drastically as a function of the target-radar configuration. Fig. 3(a) illustrates a multi-aspect, single-target system as a function of the aspect angle. The radar images of the target vary on both small and large angular scales. These changes can be understood by examining a single pixel within a set of angularly varying, co-registered, multi-aspect images. Figs. 3(b) and 3(c) are illustrations of these changes as a function of multiple regions within the MSTAR data of the T-72 at 15° depression. On the small scale, there are perturbations in pixel values for changes as small as 1°. Radar noise, error in alignment, and minor changes in viewing geometry can all contribute to variations in intensity. The significant fluctuations, however, are seen more clearly by analyzing larger angular scales. First, there is target self-occlusion. This occurs because the target-radar geometry precludes the radar from being able to image all sides of the target from a single aspect. Therefore, under certain sets of aspect angles, the intensity of particular pixels will be low because no power emitted from this area of the target can be received by the radar – this part of the target is in the shadow region. Secondly, even when features are not in the shadow, the relative geometry of features can change for varying aspects. A flat plate, for example, will exhibit its specular return when the radar aspect is perpendicular to the surface. Conversely, a sphere will have roughly uniform reflectivity regardless of aspect.

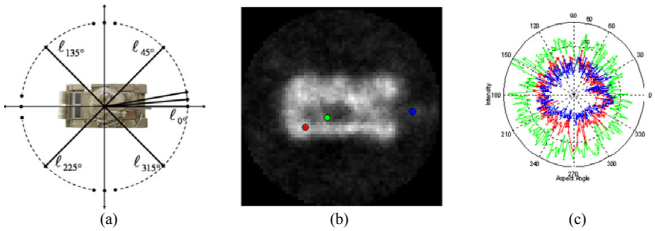

(a) (b) (c)

Fig. 3. The typical phenomenology for an aspect varying target/radar configuration, and an illustration of small and large scale angular perturbations for three pixels: (a) configuration, (b) points of interest, (c) intensity of POIs.

IEEE Catalog Number: CFP08827-CDR
ISBN: 978-1-4244-2499-3
Library of Congress: 2008903800

The proposed persistence model aims to utilize a transformation rule to convert the data from an aspect-dependent space to a new image-space. The characteristics of the target within the new persistence image-space will be dependent on the transformation function, which can either be defined outright or it can optimize a cost function. Appropriate persistence image-spaces could aid in classification, characterization of targets, scattering center extraction. The concept of a target feature, as used here, is simply a quantity that represents information of interest to an ATR algorithm. Features could therefore represent physical characteristics of the target or their respective RF signature in a SAR image. For example, an intensity-based cost function can be used to help identify the percentage of aspects in which a particular pixel is shadowed. This percentage is an indication of the geometric configuration of a target. Object height, gun articulation, vehicle damage, or the location of supplies being transported are examples of information that could be derived from this image-space. The spatial distribution of speculars and associated RCS values are additional information that could be extracted from a persistence image-space.

The persistence model is implemented under the following constraint: All of the images defined by the aspect vector Θ are pre-registered in the identical sensing space defined by I_{ℓ_n}. If the target chips are taken from a larger SAR image then detection processing and the geospatial co-registration problem has already been solved. Traditional target detection and localization algorithms often generate image chips according to the above constraint [16]. If necessary, more sophisticated registration techniques can also be applied to account for spatial registration as well as disparate image resolutions. Target centering is not required, nor is registration to a static known pose; co-registration is sufficient. The general phenomenology of a circular SAR target-radar collection configuration is displayed in Figure 3(a); for each pass of the radar, a single-aspect generates a single image. Although the development and testing consider a circular aperture, this concept can easily be expanded to work with an arbitrary collection geometry. Multiple images or sub-apertures build up the dataset to obtain information for various target poses. The set of L total aspects (or sub-apertures) is defined by the aspect vector Θ given by

$$\Theta = \{\ell_{0^\circ}, \ell_{\Delta^\circ}, ..., \ell_{(L-1)\Delta^\circ}\}. \quad (8)$$

Next, each aspect is defined by a radar image. However, instead of viewing each radar image as a 2-D image, each image is represented as a 1-D vector according to the appropriate raster scan of the individual pixels. This common representation causes no loss of generality. A target image of size $M \times N$ described by an arbitrary aspect, ℓ_n, is defined as

$$\mathrm{I}_{\ell_n} = \{x_1, x_2, ..., x_{MN}\} \quad (9)$$

where x_i represents the pixel intensity of the i^{th} indexed pixel.

In Equations (8) and (9), the data are defined as either an image in the single-aspect space or a point in the multi-aspect space. In a full dataset however, the data will be a multi-dimensional vector in a multi-dimensional aspect space. The data as viewed from its geospatial aspect dependent representation is defined by the vector $D(\ell_n, i)$,

$$D(\ell_n, i) = \begin{bmatrix} \mathrm{I}_{\ell_{0^\circ}} \\ \mathrm{I}_{\ell_{\Delta^\circ}} \\ \vdots \\ \mathrm{I}_{\ell_{(L-1)\Delta^\circ}} \end{bmatrix} = \begin{bmatrix} x_1^{\ell_{0^\circ}}, x_2^{\ell_{0^\circ}}, ..., x_{MN}^{\ell_{0^\circ}} \\ x_1^{\ell_{\Delta^\circ}}, x_2^{\ell_{\Delta^\circ}}, ..., x_{MN}^{\ell_{\Delta^\circ}} \\ \vdots \\ x_1^{\ell_{(L-1)\Delta^\circ}}, x_2^{\ell_{(L-1)\Delta^\circ}}, ..., x_{MN}^{\ell_{(L-1)\Delta^\circ}} \end{bmatrix} \quad (10)$$

where $D(\ell_n, i)$ represents the intensity of the i^{th} pixel at an aspect of ℓ_n. The transformed persistence image-space, $D^P(\rho_n, i)$, can be defined similarly as

$$D^P(\rho_n^i, i) = \begin{bmatrix} x_1^{\rho_0^1}, x_2^{\rho_0^2}, ..., x_{MN}^{\rho_0^{MN}} \\ x_1^{\rho_1^1}, x_2^{\rho_1^2}, ..., x_{MN}^{\rho_1^{MN}} \\ \vdots \\ x_1^{\rho_{L-1}^1}, x_2^{\rho_{L-1}^2}, ..., x_{MN}^{\rho_{L-1}^{MN}} \end{bmatrix}. \quad (11)$$

Notice that adjacent pixels in the aspect space come from the same initial SAR image at a given aspect angle, while adjacent pixels in the image-space can be a function of any of the initial aspect images.

The flowchart for generating a set of persistence images is given in Fig. 4. As an input, the model takes in a set of SAR images over a range of aspects. Each image is represented as a vector; those vectors are ordered as a function of the aspect angle. The persistence image-space is then defined by either a direct mapping function or the minimization of a cost function. The appropriate transformation is applied and the set of persistence images is output.

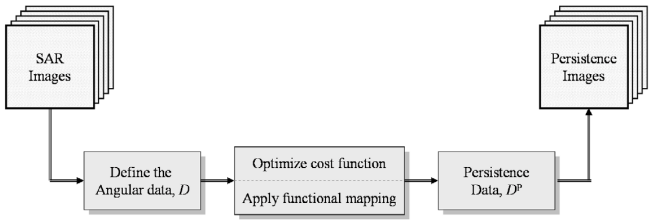

Fig. 4. The persistence model takes a set of aspect dependent images and outputs a new set of images that have a desired image-space behavior.

The purpose of the persistence transformation is to obtain the persistence vector, P^i, for the i^{th} pixel, given as

$$\mathrm{P}^i = \{\rho_0^i, \rho_1^i, ..., \rho_\alpha^i, \ldots \rho_{L-1}^i\}. \quad (12)$$

The intensity of the i^{th} pixel at a persistence level of α is given by $x_i^{\rho_\alpha^i}$ where the intensity is a function of the aspect dependent image set, i.e.

IEEE Catalog Number: CFP08827-CDR
ISBN: 978-1-4244-2499-3
Library of Congress: 2008903800

$$x_i^{\rho_\alpha^i} = \Im(D). \quad (13)$$

The mapping function $\Im(\cdot)$ can be defined by a desired image-space behavior or as the minimization of a desired cost function. An example of an outright mapping function would be to define the image-space as sub-aperture averages of the aspect space. In other words, a persistence image could represent the average of three images – an image at a central aspect, and the images directly before and after it in the aspect space. The corresponding transformation would be given as

$$x_i^{\rho_\alpha^i} = \Im(D) = \frac{1}{3}\left(D(\ell_{\alpha-1}, i) + D(\ell_\alpha, i) + D(\ell_{\alpha+1}, i)\right). \quad (14)$$

In the mapping above, the intensity of the persistence image at pixel i is a function of three aspect images at the same pixel location. The value of a persistence pixel can be defined not only as a function of aspect, but also as a function of spatial location. An alternative to directly defining a transformation function is to define a cost function $J(\cdot)$. The transformation function $\Im(\cdot)$ is defined as the function that minimizes $J(\cdot)$. An example of defining an image space via a cost function is given below. The use of direct functional transforms is well suited for problems where the image-space is defined in terms of the behavior of the aspect space images (sub-aperture images, image neighborhoods, etc…). A cost function, on the other hand, is useful in problems where the behavior of the image-space is dictated by particular constraints (minimizing separation differences, defining variance tolerances, etc…).

The first step in realizing a persistence image-space is to identify the desired behavior in the new space. For illustration, the goal of the persistence model will be to represent the intensity variations of a single pixel taken from a set of aspect varying images. Therefore, a logical method by which to define a cost function is to score the data based on the measured reflectivity. For simplicity, the persistence cost function will only consider values in the initial dataset at the identical pixel location. Since intensity variation is the main characteristic for the persistence image-space, an appropriate cost function would be to minimize the difference in reflectivity from one image to the next within the image-space. The cost function can thus be defined as

$$J(i) = \sum_{\alpha=2}^{L} \left| D^P(\rho_\alpha^i, i) - D^P(\rho_{\alpha-1}^i, i) \right|. \quad (15)$$

The i^{th} persistence vector is therefore given as

$$\{\rho_0^i, \rho_1^i, \ldots, \rho_\alpha^i, \ldots \rho_{L-1}^i\} = \{\ell_{n\Delta^\circ}, \ldots \ell_{\Delta^\circ}, \ldots, \ell_{m\Delta^\circ}\} \quad (16)$$

such that $D^P(\rho_\alpha^i, i) < D^P(\rho_{\alpha'}^i, i) \quad \forall \alpha < \alpha'$. The intensity at a given pixel in the persistence image-space is therefore a linear reordering of the initial aspect-dependent values at the identical pixel location. The range of α is determined by the total number of input images, but is normalized to [0 1].

III. Results and Conclusions

A. Fusion Based on the Matrix Fourier Transform

The fusion technique was applied to the ERADS Slicy database, a public database released in October 2004 by Expert Radar Signature Solutions (ERADS). The database is of a 1/16th scale variant of the reference model Slicy, which is a conglomerate target of canonical shapes. The base of the Slicy model is a rectangle of size 171.9 mm × 152.8 mm. The data were collected at X-Band and Ka-Band frequencies at 5° and 40° depression angles.

The image registration is a critical factor for realizing our method, because the data fusion rule assumes that the rotation center on the target is fixed when data are collected, and located at the origin of the spatial coordinate system. However, the data from the database do not satisfy this requirement, since their radar is always aimed at the bottom of the target for all aspect angles. This problem is solved by the so-called circle registration technique depicted in Fig. 5. The vector pointing from the rotation center to the origins is defined as the Rotation Vector (RV). An example of a single-aspect and fused image at Ka-band are shown in Figs. 6 and 7 respectively.

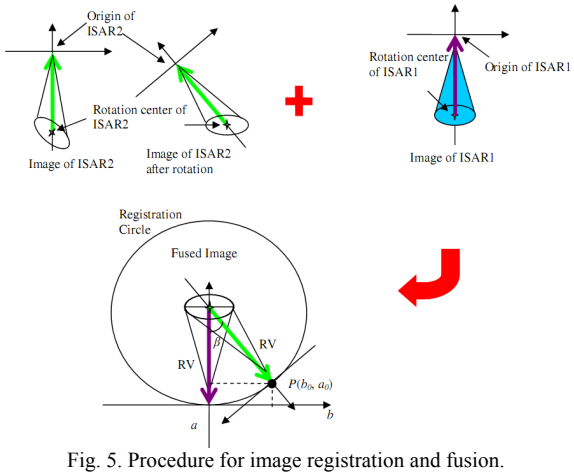

Fig. 5. Procedure for image registration and fusion.

B. Classification Based on the Persistence Model Approach

DARPA's Moving and Stationary Target Acquisition and Recognition (MSTAR) database was used for the analysis. The dataset contains spotlight SAR images of various targets at 1-foot resolution at a range of 5 km.

Fig. 8 shows the D7 bulldozer target for five values of persistence α. At $\alpha = 0$, the overall shape of the target is identified. For low values of α, the cab top and motor hutch become discernable. These features are visible over large ranges of aspects and correspond to the tallest points of the target. As the value of α increases towards 1, the aspect dependent features emerge. For example, notice at $\alpha = 1$, the returns from the plow and plow connections become visible. Such features are obfuscated and spread over many

IEEE Catalog Number: CFP08827-CDR
ISBN: 978-1-4244-2499-3
Library of Congress: 2008903800

images in the initial dataset, all of these features cannot be seen in a single image within the aspect dependent dataset. In the set of persistence images, however, these connectors and features are seen in a single image because of the intensity based transformation. Generally, the features common in all aspects (features with geometrically uniform reflectivity, features not shadowed, and features with greatest height) are seen for low values of α, but features with high reflectivity (speculars and features often hidden due to target self-occlusions) emerge when α approaches 1, regardless of pose.

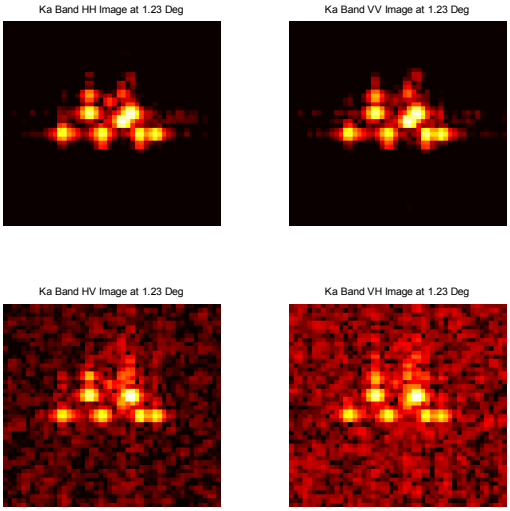

Fig. 6. Ka-band individual image centered at 1.23º aspect obtained by all polarizations at 40º depression angle.

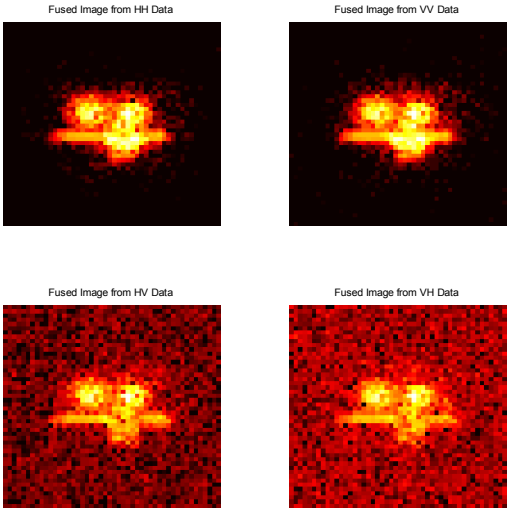

Fig. 7. Ka-band fused image obtained by all polarizations from 180 aspects at 40º depression angle.

The framework for persistence modeling transforms the set of aspect dependent images into a new image-space whose nature is defined by either a functional mapping or a cost function. Through careful definition of the transformation method, the image-space was seen to have characteristics that may be useful to a wide variety of ATR applications.

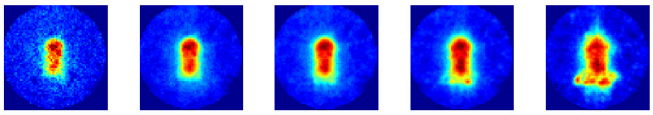

(a) (b) (c) (d) (e)

Fig. 8. Persistence model images for D7. (a) α=0, (b) α=0.25, (c) α=0.5 (d) α=0.75 (e) α=1.

REFERENCES

[1] Z. Bao, C. Sun, and M. Xing, "Time-frequency approaches to ISAR imaging of maneuvering targets and their limitations," *IEEE Trans. Aerosp. Electron. Syst.,* vol. 37, no. 3, pp. 1091-1099, July 2001.

[2] D.A. Ausherman, A. Kozma, J.L. Walker, H. M. Jones, and E.C. Poggio, "Developments in radar imaging," *IEEE Trans. Aerosp. Electron. Syst.*, vol. 20, no. 4, pp. 363-400, July 1984.

[3] C. C. Chen and H. C. Andrews, "Target-motion-induced radar imaging," *IEEE Trans. Aerosp. Electron. Syst.,* vol. 16, no. 1, pp. 2-14, January 1980.

[4] G. Wang, Z. Bao, and X. Sun, "Inverse synthetic aperture radar imaging of nonuniformly rotating targets," *Opt. Eng.*, vol. 35, no. 10, pp. 3007-3011, Oct. 1996.

[5] L.C. Trintinalia and H. Ling, "Joint time-frequency ISAR using adaptive processing," *IEEE Trans. Antennas Propagat.,* vol. 45, no. 2, pp. 221-227, Feb. 1997.

[6] V.C. Chen and S. Qian, "Joint time-frequency analysis for radar range Doppler imaging," *IEEE Trans. Aerosp. Electron. Syst.,* vol. 34, no. 2, pp. 486-499, April 1998.

[7] Z. Bao, G. Wang, and L. Luo, "Inverse synthetic aperture radar imaging of maneuvering targets," *Opt. Eng.,* vol. 37, no. 5, pp. 1582-1588, May 1998.

[8] G. Wang and Z. Bao, "Inverse synthetic aperture radar imaging of maneuvering targets based on chirplet decomposition," *Opt. Eng.,* vol. 38, no. 9, pp. 1534-1541, September 1999.

[9] A.L. Hume and C.J. Baker, "Netted radar sensing," *IEEE Aerosp. Electron. Syst. Mag.,* vol. 18, no. 2, pp. 3-6, February 2003.

[10] C.J. Baker, H.D. Griffiths, and M. Vespe, "Multi-perspective imaging and image interpretation," *Proc. NATO Advanced Study Institute on Imaging for Detection and Identification*, Il Ciocco, Italy, pp. 1-25, July-August 2006.

[11] R.L. Moses, E. Ertin, and C. Austin, "Synthetic aperture radar visualization," *Conference Record of the Thirty-Eighth Asilomar Conference on Signals, Systems and Computers*, Pacific Grove, CA, vol. 1, pp. 13-17, November 2004.

[12] M.L. Bryant, L.L. Gostin, and M. Soumekh, "3-D E-CSAR imaging of a T-72 tank and synthesis of its SAR reconstructions," *IEEE Trans. Aerosp. Electron. Syst.*, vol. 39, no. 1, pp. 211-227, January 2003.

[13] M. Soumekh, "Circular synthetic aperture radar", Chap. 7, *Synthetic Aperture Radar Signal Processing with MatLab Algorithms*, New York, NY: Wiley-Interscience, 1999.

[14] T.D. Ross and J.C. Mossing, "The MSTAR evaluation methodology," *Proc. SPIE Conf. Algorithms for Synthetic Aperture Radar Imagery VI*, Orlando, FL, pp. 702-713, April 1999.

[15] S. P. Kim, and N. K. Bose, "Reconstruction of 2-D bandlimited discrete signals from nonuniform samples," *IEE Proc. Radar and Signal Processing,* vol. 137, no. 3, pp. 197-204, June 1990.

[16] Y. Bentoutou, N. Taleb, K. Kpalma, and J. Ronsin, "An automatic image registration for applications in remote sensing," *IEEE Trans. Geosci. Remote Sens.*, vol. 43, no. 9, pp. 2127-2137, September 2005.

IEEE Catalog Number: CFP08827-CDR
ISBN: 978-1-4244-2499-3
Library of Congress: 2008903800